Understanding the grain size dependence of functionalities in lead-free (Ba,Ca)(Zr,Ti)O_3

Mao-Hua Zhang[1,2,3], Changhao Zhao[3,4,*], Xiaodong Yan[5], Shidong Wang[6,*], Shengtao Li[4], Mupeng Zheng[3,5,*], Yudong Hou[5], Wen Gong[1], Long-Qing Chen[2]

[1]Wuzhen Laboratory, Jiaxing 314500, China
[2]Department of Materials Science and Engineering, The Pennsylvania State University, University Park, PA 16802, USA.
[3]Department of Materials and Earth Sciences, Technical University of Darmstadt, Darmstadt, 64287, Germany.
[4]State Key Laboratory of Electrical Insulation and Power Equipment, Xi'an Jiaotong University, Xianning West Road 28, Xi'an, 710049, P. R. China
[5]Key Laboratory of Advanced Functional Materials, Education Ministry of China, Faculty of Materials and Manufacturing, Beijing University of Technology, Beijing, 100124, China.
[6]Musculoskeletal Tumor Center, Peking University People's Hospital, Beijing 100044, China

Abstract

Grain size effects in ferroelectric ceramics have long been exploited to tailor their functional properties. However, the underlying mechanism for the grain size effects is not yet fully understood. Here, we study the grain size dependence of domain wall activities in a lead-free piezoceramics system, (Ba,Ca)(Zr,Ti)O_3, with grain sizes in the range of 4−22 μm. The dielectric permittivity is highest at intermediate grain sizes (~12 μm) where there are moderate lattice distortion and the most active domain wall motion under low voltages. Despite the larger fraction of switched domains in the material with larger distortion (~22 μm), as revealed by *in situ* electric-field synchrotron X-ray diffraction, time-resolved characterizations demonstrate an easier and faster domain wall dynamics in the sample with moderate lattice distortion. Our analysis and phase-field simulations show that the grain size dependence of the domain wall dynamics of polycrystalline ferroelectrics is dictated by the interaction between an external electric field and the grain size-related change in intergranular stress, and this interaction is most effective in stimulating the movement of non-180° domain wall at intermediate grain sizes during the initial phase of polarization reversal. Our results provide a new fundamental understanding to guide the future design of materials for improving functionalities.

Key words: Perovskites, Lead-free electroceramics, Grain size, domain wall dynamics, High-energy X-ray diffraction, Phase-field simulations

Introduction

Crystal size effects in ferroelectric perovskites are of great fundamental and technical importance due to the continuing demand for portability in consumer electronics, the development of microelectronics and portable communication systems, which requires the miniaturization and integration of ferroelectric components. The reduction in the physical dimensions of ferroelectrics is accompanied by a drastic change in the functional properties, which dictates the extent to which ferroelectrics can be implemented in next-generation microelectronic devices [1-3].

In piezoceramics, crystal size effects are reflected in the form of grain size dependence of the crystal structure [4-7], the microstructure [8-10], and the functional properties [11, 12]. One of the well-recognized examples is found in $BaTiO_3$ bulk ceramics, exhibiting a progressive variation of dielectric, elastic, and piezoelectric properties as the grain size reduces [13]. In particular, superior dielectric and electromechanical properties are observed as the grain size approaches the critical value of ~1 μm [12]. The intriguing scaling effect has motivated numerous research activities since the 1970s, and two theoretical models have been put forward to account for the enhanced functional properties at ~1 μm from the perspective of non-180° domain wall motion [12, 14, 15] and internal residual stress [16-18].

As piezoceramics are cooled through the Curie point to develop ferroelectric order, internal stresses arise as the result of the deformation of the grains from cubic symmetry and constraint of the crystal due to polycrystallinity [16]. The stresses can be minimized by twinning (formation of non-180° domain structures), which exhibits a strong dependence on the grain size [8, 9]. Buessem *et al.* [16, 18] and Bell *et al.* [17] attributed the high permittivity in $BaTiO_3$ ceramics to increased internal residual stresses, assuming that non-180° domain switching is not present in fine-grained ceramics. This is supported by a recent study by Hennessey *et al*. [19], which shows that the pinning of domain wall motion is exacerbated near grain boundaries. It was subsequently proposed by Arlt *et al.* that the high permittivity is attributed to increased contribution of domain walls [12]. Thereafter, the domain wall motion model seems to prevail over the other in the literature. For example, Hoshina *et al.* [20, 21] showed that the non-180° domain density reaches its maximum at about 1 μm in $BaTiO_3$, which enhances the domain wall vibration and contributes to the optimal electromechanical properties. Ghosh *et al.* [15] used *in situ* synchrotron X-ray diffraction (XRD) to demonstrate that 90° domain wall motion is facilitated at subcoercive and strong electric field amplitudes, which was believed to confirm the theory of Arlt *et al.* [12, 22]. In particular, their analyses showed that no significant variation

in internal residual stress was observed over the 1–3.5 μm grain size range, suggesting that the enhanced piezoelectric properties cannot be reconciled with the residual stress theory.

However, the important role of the elastic residual stress that plays during the polarization reversal process cannot be completely omitted. Demartin and Damjanovic [23] examined the dependence of piezoelectricity on external alternating and static pressure, presenting evidence for the existence of strong internal pressure in fine-grained $BaTiO_3$ ceramics. It was found that the activity of the domain walls in the fine-grained material is much weaker than in the coarse-grained samples, since the domain walls are clamped by the high internal pressure. Daniels *et al.* [24] demonstrated a two-step process of domain reorientation. They found that the first step, characterized by a much faster time constant, is driven and facilitated by the release of a residual stress. In addition, the internal residual stress is thought to act as an auxiliary mechanical force for the initial movement of the non-180° domain [25], and it can inhibit further movement of the ferroelastic domain walls as the sample approaches a saturated poled state [26], which is consistent with the earlier study [24].

It seems that the internal stress also plays an important role in non-180° domain wall motion and should be considered when analyzing grain size dependence of functional properties. In addition to the movement of domain wall and the internal stress, the change in grain size is accompanied by the simultaneous change in other parameters that can exert profound influence on the dynamics of domain wall motion [27], including the lattice distortion [6, 28] and domain wall-grain boundary interactions [29, 30]. The existing literature focuses exclusively on the influence of grain size on the small-signal functionalities (dielectric permittivity and piezoelectric coefficients), studies on the grain size dependence of the large-signal properties and the domain wall dynamics are still scarce [15, 24, 26].

To elaborate on the influence of grain size as well as the interplay of the above two mechanisms and their effects on the switching behavior of polycrystalline materials, we investigated a series of lead-free $(Ba,Ca)(Zr,Ti)O_3$ (BCZT) samples with a single-phase tetragonal structure and grain sizes in the range of 4–22 μm. There are two reasons for choosing the BCZT system. First, the grain size of the materials can be easily adjusted without having to use different sintering methods. Second, BCZT proves to be a promising lead-free piezoceramic system due to its excellent piezoelectric and ferroelectric properties. The large-signal macroscopic dielectric and piezoelectric measurements are complemented by small-signal field-dependent dielectric permittivity in the subcoercive field regime, *in situ* field-dependent high-energy X-ray diffraction (XRD), time-dependent characterization of the domain wall

dynamics at higher electric fields, and phase-field simulations of the domain switching behavior under mechanical stress.

Experimental Section

$0.4Ba(Zr_{0.2}Ti_{0.8})O_3$-$0.6(Ba_{0.7}Ca_{0.3})TiO_3$ (BZT-60BCT) ceramic samples with different grain sizes were prepared by the conventional solid-state reaction method using ultrafine nanopowder prepared by high-energy ball milling and a two-step sintering procedure, as described elsewhere [31]. The dwelling time in the first and second stages was set at 1 min and 6 h, respectively. The temperature was rapidly decreased from T_1 to T_2, and the temperatures in the two stages were adjusted to produce ceramics with different grain sizes, as listed in Supplementary Table 1. The bulk density of ceramics was measured by the Archimedes principle using a density meter (XS104, Mettler Toledo, Switzerland). With a theoretical density of 5.668 g/cm^3, the relative density and porosity of the investigated samples are listed in Supplementary Table 1. Since the compositions studied do not contain volatile elements, the chemical compositions of the ceramic samples with different grain sizes are considered to be uniform. We note that a minor amount of a nonperovskite secondary phase was detected in all samples after sintering. The amount of this phase was too small for reliable identification, but it is likely that its composition is close to $CaTiO_3$. Due to the very small amount, nominal compositions are used in the manuscript. The microstructure of the studied samples was examined using a scanning electron microscope (SEM, S4800, Hitachi, Japan). Before measurement, the cross-sections of the ceramics were polished using diamond paste and then thermally etched for 10 min at temperatures of 1200-1275 °C, depending on the sintering temperature. The average grain size (**Figure S1**) was estimated using the line intercept method and Nano Measurer software. Detailed descriptions of the preparation and characterization of the transmission electron microscope (TEM) results are found in Ref. [31].

The investigated samples were sputtered with platinum electrodes for all electrical measurements. For the measurement of the piezoelectric charge coefficient, d_{33}, and the planar electromechanical coupling factor, k_p, the samples were poled under a DC electric field of 4 kV/mm at 40 °C for 30 min in a silicone oil bath. Temperature and frequency dependence of the dielectric permittivity were measured using an impedance analyzer (4192A LF, Hewlett-Packard, USA) during a heating cycle at a rate of 2 °C/min on the unpoled samples. Field dependence of the dielectric permittivity in the subcoercive field regime was performed on the poled samples using an impedance analyzer (Alpha-Analyzer, Novocontrol, Germany) connected to a high-voltage unit (HVB 300, Novocontrol, Germany). A sinusoidal AC field of 0-120 V/mm with a frequency of 1 kHz was applied.

Large-signal polarization and strain hysteresis loops were measured using a modified Sawyer-Tower circuit equipped with an optical displacement sensor (D63, Philtec Inc., USA),

and a bipolar electric field of 2 kV/mm at 0.1 Hz was applied. Detailed descriptions of the pulse switching setup and its mechanisms are found elsewhere [26]. Annealed samples (annealing at 400 °C for 1 h) were subjected to a bipolar electric field of 2 kV/mm at 0.5 Hz and cycled 20 times to remove any unstable electric contributions prior to polarization switching measurements. The time dependence of the switched polarization was recorded under a wide range of applied electric field pulses, E_{Sw}, ranging from 40 V/mm to 900 V/mm. Prior to each measurement, the samples were poled at 2 kV/mm for 10 s, followed by a relaxation time of 30 s. Afterwards, a sequence of electric fields of increasing field amplitude was applied, including a switching and a reference measurement. Note that the sample's response on the fast time domain (10^{-6} s ~ $5{\cdot}10^{-4}$ s) was measured by an oscilloscope (Agilent MSO7014B, Santa Clara, CA, USA), while the slow time domain (>10^{-4} s) was recorded by a measurement card (USB-6211, National instruments, Austin, TX, USA). The non-switching contributions from dielectric displacement and leakage current were subtracted. Large-signal polarization and strain hysteresis loops were measured at 2 kV/mm and 0.1 Hz before and after each polarization switching measurement to ensure that no irreversible change in properties was induced during the pulse measurement.

The high-energy diffraction patterns were collected at The European Synchrotron Radiation Facility (ESRF) beamline ID15A in transmission geometry with a Pilatus 2M CdTe area detector (Dectris Ltd., Switzerland) placed at a distance of 600 mm from the sample to collect diffraction data. The beam energy was 60 keV at a wavelength of 0.20664 Å and the spot size was set at 0.244 × 0.244 mm^2. The sample was placed in a sample stage specially designed for *in situ* field measurements [32] and immersed in silicone oil. During the measurement, the unpoled samples were subjected to two successive cycles of a bipolar electric field of 2 kV/mm at a frequency of 0.025 Hz, with the frame exposure time set at 500 ms.

The beam center and tilt were refined using the DIOPTAS program [33] for each pattern with respect to a standard diffraction pattern of CeO_2 taken under the same settings. The Debye-Scherrer diffraction rings obtained from the samples were divided into azimuthal sectors of 10° width and the patterns within each sector were integrated to obtain equivalent diffraction intensities as a function of 2θ using the Fit2D program [34], respectively. The directional difference between the scattering vector, Q, of each sector and the applied field, E, is denoted by ψ (the corresponding sector is called ψ-sector).

Rietveld refinement of the high-energy XRD patterns of the samples in the unpoled state was performed using the GSAS program [35]. The initial parameters of the *P*4*mm* model for the refinement were taken from the XRD data refinements of Buttner and Maslen [36]. For the

analysis of elastic residual strains, the 111 reflections (hereafter the hkl indexes are based on the pseudocubic coordinate system with the unit vector |a| ≈ 4 Å) of the studied samples were fitted with a one-peak model with Gaussian profile using LIPRAS [37]. The peak position of each sector in the remanent state is taken as a reference in each sector to calculate the *d*-spacing values based on Bragg's law. This allows us to calculate the change of the residual strain with respect to the remanent state as a function of electric field.

Phase-field simulations were performed on a two-dimensional system discretized into square meshes with a mesh size of 1.0 × 1.0 nm for the numerical simulation. A periodic boundary condition was employed. For the simulation of domain structures, the stress-free condition is used, which assumes that the averaged stress of the simulated system is zero. For the simulation of polarization and strain hysteresis loops, the strain-free condition assuming that the averaged strain is zero is adopted. The temporal evolution of the polarization field $\mathbf{P}(\boldsymbol{r},t)$ is described by the time-dependent Ginzburg-Landau (TDGL) equation [38]:

$$\frac{\partial \mathbf{P}}{\partial t} = -L_P \frac{\partial F}{\partial \mathbf{P}} \tag{2}$$

where L_P is the kinetic coefficient, $\boldsymbol{r}$ is the space position, t is the time, and F is the total free energy of the system, which is formulated as the sum of the Landau free energy, the electrostatic free energy, the elastic energy, and the gradient energy, namely, $F = F_{\text{Landau}} + F_{\text{electrostatic}} + F_{\text{elastic}} + F_{\text{gradient}}$. The equations of the above free energies are given elsewhere [38, 39]. The material coefficients used in the present work, including the Landau coefficients, the elastic stiffness, the electrostrictive coefficients, the gradient energy coefficients, and the background dielectric permittivity are listed in Supplementary Table. 2. The domain switching behavior is investigated under a uniaxial compressive stress of 134 MPa, a uniaxial tensile stress of 134 MPa, and stress-free conditions, simulating the residual stresses of grains embedded in piezoceramics. Taking the Young's modulus of $BaTiO_3$ bulk of 67 GPa, a compressive/tensile stress of 134 MPa corresponds to a nominal compressive/tensile strain of 0.2%.

Results and Discussion

The nominal composition of the studied materials is $0.4Ba(Zr_{0.2}Ti_{0.8})O_3$-$0.6(Ba_{0.7}Ca_{0.3})TiO_3$ (BZT-60BCT) which is a tetragonal structure and away from the morphotropic phase boundary at BZT-50BCT [40]. The details of the materials with different grain sizes are described in the "Methods" section. The grain size dependence of the small-signal dielectric and piezoelectric properties of the investigated BCZT ceramics is demonstrated in **Figure 1a**. An increase in the dielectric permittivity, $\varepsilon_{33}/\varepsilon_0$, piezoelectric coefficient, d_{33}, and electromechanical coupling factor, k_p, is observed as the grain size increases from 4 μm to 12 μm. Despite a further slight increase in both k_p and d_{33} with increasing grain size from 12 μm to 22 μm, the dielectric permittivity reaches its maximum at 12 μm and decreases with increasing grain size. Three selected samples with an average grain size of 4 μm, 12 μm, and 22 μm (abbreviated as G4, G12, and G22, respectively) are therefore chosen for detailed electrical and structural characterizations under large electric fields in the following. The temperature dependence of the dielectric permittivity and loss tangent of G4, G12, and G22 samples is depicted in **Figure S2**. The Curie points of the three samples studied are very close to each other, being 88 °C, 89 °C, and 90 °C for the G4, G12, and G22 samples, respectively. The slight increase in the Curie point with increasing grain size is because the lattice distortion increases in materials with larger grain sizes (**Figure 1d**), obtained from the Rietveld refinement of the high-energy X-ray diffraction (XRD) patterns of the materials studied (**Figure S3**).

The different permittivity values can be associated with the activity of the domain wall motion under low excitation voltages [21], and the field dependence of the dielectric permittivity under subcoercive field conditions is depicted by the Rayleigh model (**Figure 1b**), $\varepsilon(E) = \varepsilon_{init} + \alpha_\varepsilon E$, where $\varepsilon(E)$ is the field-dependent permittivity, ε_{init} is the initial permittivity, and α_ε is the Rayleigh coefficient [41, 42]. The irreversible domain wall motion occurs when the applied force is sufficiently large to overcome the potential barrier separating two local energy minima [43] and the Rayleigh coefficient characterizes the contribution from irreversible domain wall motion to the dielectric permittivity. The Rayleigh coefficient α_ε of the G12 sample is 11.7 mm/V, which is larger than that of the G4 sample (9.5 mm/V) and the G22 sample (5.2 mm/V). Under weak field conditions, there is no switching of domain walls or nucleation of new walls [43], and the external field causes only vibrations or small irreversible displacements of the domain walls [44]. Thus, the highest α_ε value for the G12 sample is due to the most active domain wall movement in the range of electric fields below the coercive field.

The ferroelectric and piezoelectric responses of samples exposed to higher electric fields are revealed by the macroscopic polarization (**Figure 1c**) and strain hysteresis loop (**Figure S4**).

The same coercive field of 0.22 kV/mm is observed for the G4 and G12 samples, and the G22 sample has a larger coercive field of 0.30 kV/mm. The maximum polarization is 11.2 μC/cm^2, 12.8 μC/cm^2, and 12.7 μC/cm^2 for the G4, G12, and G22 samples, respectively. A remanent polarization of 3.6 μC/cm^2 and 5.5 μC/cm^2 is observed for the G4 and G12 samples, respectively. While the G12 sample shows the largest small-signal permittivity, the largest remanent polarization of 6.2 μC/cm^2 is found for the G22 sample. The G12 sample exhibits the highest positive strain of 0.072% at 2 kV (**Figure S4**), while a positive strain of 0.063% and 0.058% are found in the G22 and G4 sample, respectively.

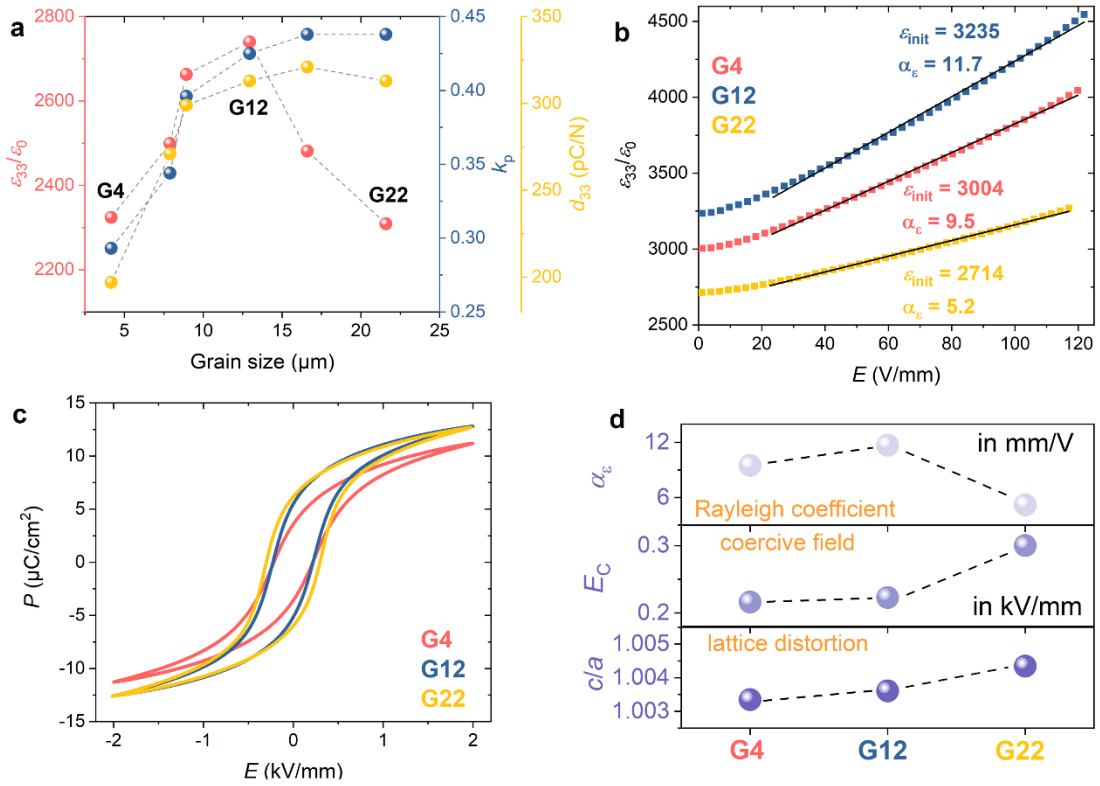

Figure 1. **a** Grain size dependence of dielectric permittivity, $\varepsilon_{33}/\varepsilon_0$ (@ 1 kHz), electromechanical coupling factor, k_p, and piezoelectric coefficient, d_{33}, of the poled BCZT samples [31], measured at room temperature. **b** Field dependence of the dielectric permittivity, $\varepsilon_{33}/\varepsilon_0$, of the unpoled G4, G12, and G22 samples under subcoercive field conditions. **c** Polarization hysteresis loops of the unpoled G4, G12, and G22 samples at 0.1 Hz. **d** Grain size dependence of Rayleigh coefficient, coercive field, E_C, and tetragonal lattice distortion c/a for the unpoled BCZT samples.

Detailed structural changes of the materials of interest exposed to high electric fields were revealed using *in situ* field synchrotron XRD. All samples are characterized by the tetragonal *P*4*mm* structure in the virgin state (**Figure S3**). The contour plots of the 004/400 reflections of the G12 sample subjected to a bipolar electric field of 2 kV/mm at 0.025 Hz are shown in **Figure 2a**, and an intensity interchange of the two reflections is observed, indicative of non-

180° domain switching [45, 46]. The fraction of switched domains, η_{002}, for tetragonal perovskites can be quantified using the following equation [46]:

$$\eta_{002} = \frac{f_{002}}{3} - \frac{1}{3} = \frac{\frac{I_{002}}{I'_{002}}}{\frac{I_{002}}{I'_{002}} + 2 \times \frac{I_{200}}{I'_{200}}} - \frac{1}{3} \quad (1)$$

where f_{002} is the multiple of the 002-oriented domain fraction with respect to the unpoled state with a random distribution, I_{hkl} and I'_{hkl} represent the integrated intensity of the *hkl* reflection of interest and the unpoled reference state, respectively. The directional difference between the scattering vector *Q* and the applied field *E* is called *the* ψ-sector, varying between 0° and 90°. The η_{002} of the investigated samples from the 0°-sector, the 45°-sector, and the 90°-sector as function of electric field is featured in **Figure 2b-2d**, respectively. The η_{002} in the 45°-sector is nearly zero for three samples, indicating that the domain texture is least affected for the domains whose [001] direction is 45° away from the field direction. The η_{002} in the 0°-sector increases with increasing electric field, reaching a value of 0.12, 0.21, and 0.30, respectively, at 2 kV/mm. The above results indicate that with sufficiently large electric fields, more domains can be switched along the field direction as the grain size increases.

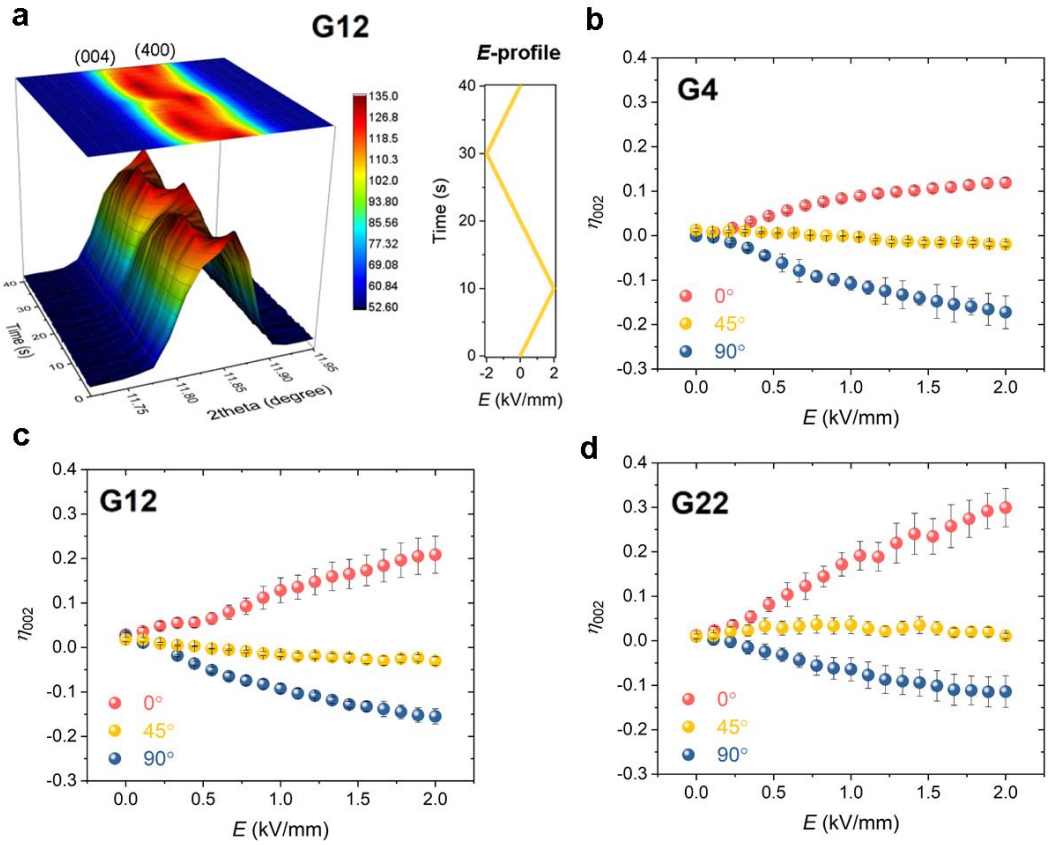

Figure 2. Contour plots of the $(004)_{pc}/(400)_{pc}$ reflections of the **a** G12 sample during the application of a bipolar electric field of 2 kV/mm at 0.025 Hz as an example to illustrate the domain switching. Shown on the right is a time-electric field (E) profile. η_{002} of the **b** G4, **c** G12, and **d** G22 samples with increasing field in directions at 0°, 45°, and 90° to the electric field.

As demonstrated in other polycrystalline ferroelectrics, including La-doped $PbTiO_3$ [47, 48], $BiFeO_3$-$PbTiO_3$ [49, 50], $(K,Na)NbO_3$ [51], and $(Ba,Ca)(Zr,Ti)O_3$ [52], domain switching usually becomes more difficult with increasing lattice distortion. However, this does not appear to be consistent with current observations, i.e., domain wall motion is more pronounced in compositions with increased lattice distortion, at least at a large electric field of 2 kV/mm, which is 7−9 times the coercive field. Nevertheless, the domain wall motion should be evaluated based on thermodynamics and kinetics. The former is determined by the maximum degree of domain wall motion in the equilibrium state under a sufficiently large electric field, while the latter is evaluated by the response rate of the domain walls to the applied electric field. The *in situ* field XRD was performed under a low-frequency electric field almost 10 times the coercive field, so that most of the domain walls had sufficient time and driving force to respond. Therefore, the XRD results evaluate the domain switching behavior mostly from the perspective of thermodynamics, i.e., the volume fraction of domains that can be switched in the millisecond range at 2 kV/mm. To better understand the domain switching behavior from the perspective of kinetics, i.e., how fast the domain walls move in response to an electric field (also known as domain wall dynamics), the time dependence of the switched macroscopic polarization was measured over a broad range of applied electric field pulses (**Figure S5**).

The switched polarization on the logarithmic time scale under the electric field of 120 V/mm (~half of the coercive field) for the three samples is featured in **Figure 3a**. Switching of piezoceramics consists of a sequence of individual events, which can be divided into three regimes [26, 51, 53]. The first regime that occurs below the coercive field is the initial non-180° domain wall motion [26]. The fastest non-180° domain wall dynamics of the G12 sample at 120 V/mm among the three samples is evidenced by its fastest polarization rise (**Figure 3a**). In contrast, the G4 and G22 samples are characterized by a slower polarization increase due to limited domain wall motion, although the G4 sample is marginally faster, as shown in the inset.

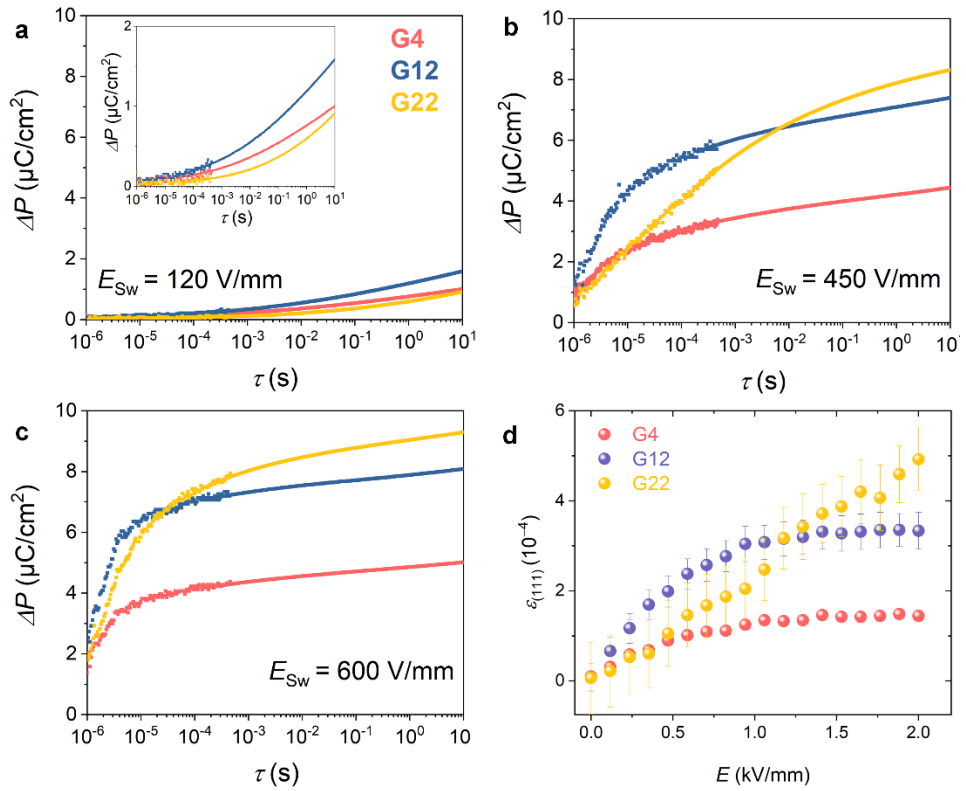

Figure 3. Grain size dependence of time-dependent polarization reversal behavior under different applied constant electric fields, E_{Sw}, of **a** 120 V/mm, **b** 450 V/mm, and **c** 600 V/mm. The sample's response on the fast time domain (10^{-6} s ~ $5{\cdot}10^{-4}$ s) was measured by an oscilloscope, while the slow time domain (>10^{-4} s) was recorded by a measurement card (see details in the "Methods" section). **d** Field-dependence of the 111 lattice strains along the field direction for the G4, G12, and G22 samples, calculated based on *in situ* synchrotron characterizations.

At 450 V/mm, ~2 times the coercive field (**Figure 3b**), the G12 sample begins with the highest initial polarization at 10^{-6} s and shows a faster polarization reversal below 10^{-3} s, where it almost enters the saturation regime, indicated by a linear increase in polarization on the logarithmic time scale [26]. The G4 sample exhibits a slower polarization increase and the slope of the ΔP-τ curve for the G4 sample decreases with time, indicating that the domain wall motion is suppressed compared to the G12 sample. The polarization increase of the G4 sample enters the linear range at ~10^{-2} s and a polarization value of 4.4 μC/cm^2 is reached at 10 s, which is 68% lower than that of the G12 sample (7.4 μC/cm^2). The G22 sample exhibits the lowest initial polarization at 10^{-6} s, and the slope of its ΔP-τ curve is smaller than that of the G12 sample before the G12 sample enters the saturation regime. This indicates that the G12 sample is characterized by a facilitated domain wall motion in the initial stages. The polarization increase of the G22 sample exceeds that of the G12 sample at ~10^{-2} s and does not enter the saturation

regime at 450 V/mm during the investigated time period, which can be attributed to the largest lattice distortion and coercive field of the G22 sample.

The behavior of the domain wall dynamics at a larger electric field of 600 V/mm (~3 times the coercive field) is highlighted in **Figure 3c**. The G4 sample shows suppressed domain wall motion, as evidenced by the slowest polarization increase and the lowest polarization value at 10 s. The G12 sample is characterized by a faster polarization increase before 10^{-5} s, where the polarization increase of the G22 sample exceeds that of the G12 sample as the latter approaches the saturation regime. In contrast, the switched polarization of the G22 sample continues to increase with time and enters the linear regime only after ~10^{-2} s, which is the latest compared to the G4 and G12 samples (between 10^{-4} s and 10^{-3} s). A polarization value of 9.3 μC/cm^2 is obtained for the G22 sample at 10 s, which is slightly higher than that of the G12 sample (8.1 μC/cm^2). Despite the largest switchable polarization in the G22 sample, as confirmed by both switching dynamics measurements and synchrotron characterizations (**Figure 2**), the G12 sample is characterized by faster and facilitated domain wall motion in the initial phase of polarization reversal. The coercive field is often used to measure how the domains of ferroelectrics with the same crystal structure can reorient under an external electric field. In most piezoceramics, the coercive field is located approximately where the negative strain is greatest [26]. The coercive fields of piezoceramics are consistently reported to be lower for ferroelectrics with smaller lattice distortion [53]. As shown in **Figure 1d**, the coercive field and lattice distortion increase with increasing grain size. The coercive field represents a macroscopic expression of the movement of domain wall and can be understood as the "activation energy" required to start the movement on the large scale. Domain wall activity is subject to various influencing parameters, including the local electric and mechanical boundary conditions, lattice distortion, grain size, and crystal structure, etc. The interaction of the above parameters determines the domain wall activity and thus the coercive field of piezoceramics.

Previous study showed that each grain is located in a unique local environment in terms of intergranular misorientations [54]. The neighboring grains with different orientations in polycrystalline ceramics are mechanically interlocked, giving rise to intergranular stress due to an adaptation of compatibility strains [45]. It has been demonstrated both theoretically [55, 56] and experimentally [57-59] that such intergranular interactions can significantly affect the ferroelectric domain switching behavior. For tetragonal perovskite systems, the intergranular stress can be evaluated by the residual lattice strains in <111>-oriented grains, since the strain contributed by non-180° domain wall movement is zero in the absence of the constraint from neighboring grains [45]. The 111 lattice strains obtained from the 0°-sector during the

polarization reversal process of the G4, G12, and G22 samples are shown in **Figure 3d**. The G12 sample shows a faster increase in lattice strain with increasing electric field at lower fields (less than 1 kV/mm) than the G4 and G22 samples and exhibits a plateau at higher fields approaching the saturated regime. The lattice strain of the G22 sample increases with increasing electric field and no saturation is observed in the investigated field range. The faster increase in the tensile strain of the G12 sample in the initial stage of domain switching is believed to be associated with a faster redevelopment of mechanical stress and hints at a faster movement of domain wall, although the switchable polarization is larger in the G22 sample. The distribution of the lattice strain as a function of the angle ψ at selected electric fields is illustrated in Figure S6. At 0.5 kV/mm, tensile strains of 0.68×10^{-4}, 1.70×10^{-4}, and 1.15×10^{-4} are measured in the 0°-sector for the G4, G12, and G22 samples, respectively. At 2.0 kV/mm, tensile strains of 1.44×10^{-4}, 3.33×10^{-4}, and 5.03×10^{-4} are measured in the 0°-sector for the G4, G12, and G22 samples, respectively. From the lattice strain change, it can be inferred that more domain wall activity of the G12 sample can be induced by applying an electric field of 0.5 kV/mm, while the application of a larger field of 2.0 kV/mm triggers more domain wall activity in the G22 sample. This suggests that the G12 sample is more responsive to the applied field in the initial phase of the polarization reversal. The overall negligible change in the lattice strain in all sectors for the G4 sample with respect to the G12 and G22 samples implies that the domain wall activity is strongly suppressed in the G4 sample, as also revealed by the above dynamics and synchrotron characterizations.

Daniels *et al.* [24] demonstrated that residual tensile strains can promote the backward motion of domain walls relative to the initial poling direction, with the corresponding compressive stress acting as an auxiliary mechanical force to facilitate the movement of non-180° domain wall [26]. Phase-field simulations were carried out to validate the effect of mechanical stress on the domain switching behavior of ferroelectric materials, as illustrated in **Figure 4a**. It essentially simulates the experimental characterization of the time-resolved polarization changes, taking into account the mechanical stress [26]. First, the material studied is poled with a large electric field along one direction to ensure polarization saturation. After poling, the material is relaxed for sufficient time steps to reach equilibrium. The switching behavior is examined by applying an electric field opposite to the poling electric field under uniaxial compressive stress, uniaxial tensile stress, and stress-free conditions, as described in "Methods" sections, simulating stress conditions for the grains embedded in piezoceramics.

As can be seen in **Figure 4b** and **Figure 4c**, the material studied exhibits a faster increase in polarization when subjected to a compressive stress. At 400 V/mm, the material under

compressive stress approaches the saturation regime with a switched polarization of ~50 μC/cm^2, while the switched polarization under a tensile stress is significantly lower (~10 μC/cm^2). At 500 V/mm, the material under a compressive stress reaches the saturation regime much earlier than the material under stress-free and tensile stress conditions. The polarization vectors during polarization reversal are illustrated at selected time steps of 0, 30,000, and 60,000 (**Figure 4d**). The material was initially polarized along the +*x* direction and then an opposite electric field was subsequently applied along the −*x* direction. Higher density of non-180° domains is observed at step 30,000. The polarization reversal of piezoceramics consists of the initial non-180° switching and subsequent 180° domain switching events [26, 53]. Both types of domains are ferroelectric and respond to external electric fields, while the non-180° domains are ferroelastic and can therefore be moved by an external mechanical field. The application of a compressive stress enhances the domain wall dynamics by facilitating the movement of non-180° domain walls. The simulation results support the hypothesis that the compressive stress, which is acting to compress the sample along the field direction, provides a driving force for the backward motion of domain walls relative to the poling direction.

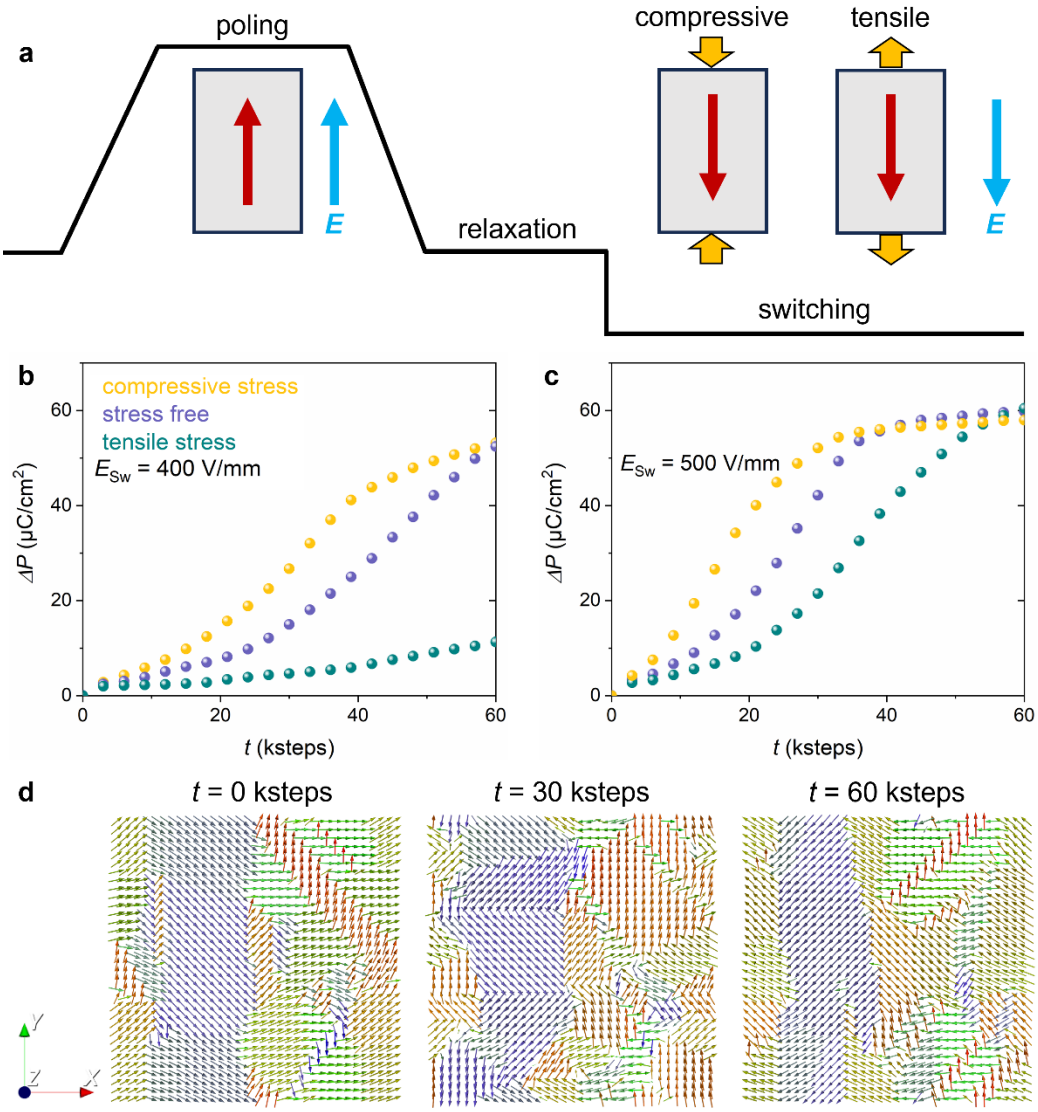

Figure 4. **a** Schematic of the electric field sequence to study the polarization switching dynamics using phase-field simulations. Time-dependent polarization reversal behavior under compressive stress, tensile stress, and stress-free conditions at **b** 400 V/mm and **c** 500 V/mm. **d** Polarization vectors of the material at selected time steps during the domain switching process.

Conclusion

To sum up, we investigate the impact of grain size on the functional properties of a prototype lead-free piezoceramics system using advanced domain wall dynamics measurements, *in situ* synchrotron XRD characterizations, and phase-field simulations. The dielectric permittivity is maximized at intermediate grain size of ~12 μm, resulting from the most active domain wall movement under small electric fields. The lattice distortion of the materials studied increases with increasing grain size. Although the lattice distortion determines how much polarization can be switched based on thermodynamics, the time-resolved domain wall dynamics measurement reveals a faster and easier movement of the domain walls in the

material with intermediate grain sizes due to the competing interaction between residual stress, intergranular stress, and applied electric fields, which is maximized at intermediate grain sizes and stimulates the initial phase of polarization reversal, i.e., non-180° domain wall motion. Phase-field simulations indicate that the facilitated switching behavior of the piezoceramics is due to the possible presence of residual compressive stress, which provides an auxiliary mechanical force to facilitate the movement of domain walls. As the field increases, the intergranular stress also increases due to the increased fraction of switched domains and the associated increase in strain, which suppresses further movement of domain walls. The interaction between residual stress and intergranular stress is subject to the change in grain size. A larger grain size leads to a lower residual stress, resulting in a slower response of the domain wall in the initial stage, while the intergranular stress also develops more slowly, so that the saturated switched domain fraction can be higher. On the other hand, a smaller grain size may lead to a faster response of the domain wall in the initial stage, but the intergranular stress also develops faster, suppressing the switched domain fraction at saturation. Our results show that targeted grain size engineering is a powerful tool for improving functional properties, as evidenced by the 59% and 45% increase in piezoelectric coefficient and electromechanical coupling factor, respectively, by adjusting the grain size from 4 μm to 12 μm. Our study shows the grain size-induced change in the functionalities is determined by the interaction between intergranular stress and electric fields.

Acknowledgement

The preparation of bulk materials and fundamental electrical characterization are supported by Beijing Natural Science Foundation (Grant No. JL23004 to M.P.Z.) and National Natural Science Foundation of China (Grant No. 52272103 to Y.H.). Other experimental efforts are supported by the Hessian State Ministry for Higher Education, Research and the Arts under the LOEWE collaborative project FLAME (Fermi level engineering of antiferroelectric materials for energy storage and insulation systems) of Germany. S.W. acknowledges the support from Beijing Natural Science Foundation (Grant No. L222066) and Peking university people's Hospital research and development funds (RS2021-04 and RDJP2022-44). We acknowledge the European Synchrotron Radiation Facility (ESRF) for the provision of experimental facilities. The synchrotron studies were carried out at the beamline ID15 under proposal number MA 4993. Phase-field simulation effort is supported by the Computational Materials Sciences Program funded by the National Science Foundation (NSF) through Grant No. DMR- 2133373 (MHZ and LQC). M.-H. Zhang thanks Jan Schultheiß for valuable discussions during the preparation of the manuscript.

References

[1] J. Junquera, P. Ghosez, Critical thickness for ferroelectricity in perovskite ultrathin films, Nature 422(6931) (2003) 506-509.

[2] D.D. Fong, G.B. Stephenson, S.K. Streiffer, J.A. Eastman, O. Auciello, P.H. Fuoss, C. Thompson, Ferroelectricity in Ultrathin Perovskite Films, Science 304(5677) (2004) 1650-1653.

[3] P. Gao, Z. Zhang, M. Li, R. Ishikawa, B. Feng, H.-J. Liu, Y.-L. Huang, N. Shibata, X. Ma, S. Chen, J. Zhang, K. Liu, E.-G. Wang, D. Yu, L. Liao, Y.-H. Chu, Y. Ikuhara, Possible absence of critical thickness and size effect in ultrathin perovskite ferroelectric films, Nat. Commu. 8(1) (2017) 15549.

[4] K. Uchino, E. Sadanaga, T. Hirose, Dependence of the Crystal Structure on Particle Size in Barium Titanate, J. Am. Ceram. Soc. 72(8) (1989) 1555-1558.

[5] T. Hoshina, H. Kakemoto, T. Tsurumi, S. Wada, M. Yashima, Size and temperature induced phase transition behaviors of barium titanate nanoparticles, Journal of Applied Physics 99(5) (2006) 054311.

[6] T. Leist, K.G. Webber, W. Jo, E. Aulbach, J. Rödel, A.D. Prewitt, J.L. Jones, J. Schmidlin, C.R. Hubbard, Stress-induced structural changes in La-doped BiFeO3–PbTiO3 high-temperature piezoceramics, Acta Mater. 58(18) (2010) 5962-5971.

[7] J. Koruza, P. Groszewicz, H. Breitzke, G. Buntkowsky, T. Rojac, B. Malič, Grain-size-induced ferroelectricity in $NaNbO_3$, Acta Mater. 126 (2017) 77-85.

[8] W. Cao, C.A. Randall, Grain size and domain size relations in bulk ceramic ferroelectric materials, J. Phys. Chem. Solids 57(10) (1996) 1499-1505.

[9] G. Arlt, Twinning in ferroelectric and ferroelastic ceramics: stress relief, Journal of Materials Science 25(6) (1990) 2655-2666.

[10] M.J. Hoffmann, M. Hammer, A. Endriss, D.C. Lupascu, Correlation between microstructure, strain behavior, and acoustic emission of soft PZT ceramics, Acta Mater. 49(7) (2001) 1301-1310.
[11] C.A. Randall, N. Kim, J.P. Kucera, W.W. Cao, T.R. Shrout, Intrinsic and extrinsic size effects in fine-grained morphotropic-phase-boundary lead zirconate titanate ceramics, J. Am. Ceram. Soc. 81(3) (1998) 677-688.
[12] G. Arlt, D. Hennings, G.D. With, Dielectric properties of fine-grained barium titanate ceramics, J. Appl. Phys. 58(4) (1985) 1619-1625.
[13] K. Kinoshita, A. Yamaji, Grain-size effects on dielectric properties in barium titanate ceramics, J. Appl. Phys. 47(1) (1976) 371-373.
[14] T. Hoshina, K. Takizawa, J. Li, T. Kasama, H. Kakemoto, T. Tsurumi, Domain Size Effect on Dielectric Properties of Barium Titanate Ceramics, Jpn. J. Appl. Phys. 47(9) (2008) 7607-7611.
[15] D. Ghosh, A. Sakata, J. Carter, P.A. Thomas, H. Han, J.C. Nino, J.L. Jones, Domain Wall Displacement is the Origin of Superior Permittivity and Piezoelectricity in $BaTiO_3$ at Intermediate Grain Sizes, Adv. Funct. Mater. 24(7) (2014) 885-896.
[16] W.R. Buessem, L.E. Cross, A.K. Goswami, Phenomenological Theory of High Permittivity in Fine-Grained Barium Titanate, J. Am. Ceram. Soc. 49(1) (1966) 33-36.
[17] A.J. Bell, A.J. Moulson, L.E. Cross, The effect of grain size on the permittivity of BaTiO3, Ferroelectrics 54(1) (1984) 147-150.
[18] W.R. Buessem, L.E. Cross, A.K. Goswami, Effect of Two-Dimensional Pressure on the Permittivity of Fine- and Coarse-Grained Barium Titanate, J. Am. Ceram. Soc. 49(1) (1966) 36-39.
[19] G. Hennessey, T. Peters, P. Tipsawat, M. Checa, L. Collins, S. Trolier-McKinstry, Domain wall motion across microstructural features in polycrystalline ferroelectric films, Acta Mater. 250 (2023) 118871.
[20] T. Hoshina, K. Takizawa, J. Li, T. Kasama, H. Kakemoto, T. Tsurumi, Domain size effect on dielectric properties of barium titanate ceramics, Jpn. J. Appl. Phys. 47(9S) (2008) 7607.
[21] T. Hoshina, Y. Kigoshi, S. Hatta, H. Takeda, T. Tsurumi, Domain Contribution to Dielectric Properties of Fine-Grained $BaTiO_3$ Ceramics, Jpn. J. Appl. Phys. 48(9) (2009) 09KC01.
[22] G. Arlt, N.A. Pertsev, Force constant and effective mass of 90° domain walls in ferroelectric ceramics, J. Appl. Phys. 70(4) (1991) 2283-2289.
[23] M. Demartin, D. Damjanovic, Dependence of the direct piezoelectric effect in coarse and fine grain barium titanate ceramics on dynamic and static pressure, Appl. Phys. Lett. 68(21) (1996) 3046-3048.
[24] J.E. Daniels, C. Cozzan, S. Ukritnukun, G. Tutuncu, J. Andrieux, J. Glaum, C. Dosch, W. Jo, J.L. Jones, Two-step polarization reversal in biased ferroelectrics, J. Appl. Phys. 115(22) (2014) 224104.
[25] P. Gerthsen, G. Kruger, Coercive field in fine-grained plzt ceramics, Ferroelectrics 11(1) (1976) 489-492.
[26] J. Schultheiß, L. Liu, H. Kungl, M. Weber, L. Kodumudi Venkataraman, S. Checchia, D. Damjanovic, J.E. Daniels, J. Koruza, Revealing the sequence of switching mechanisms in polycrystalline ferroelectric/ferroelastic materials, Acta Mater. 157 (2018) 355-363.
[27] J. Schultheiß, G. Picht, J. Wang, Y.A. Genenko, L.Q. Chen, J.E. Daniels, J. Koruza,

Ferroelectric polycrystals: Structural and microstructural levers for property-engineering via domain-wall dynamics, Prog. Mater Sci. 136 (2023) 101101.
[28] X. Li, W.-H. Shih, Size Effects in Barium Titanate Particles and Clusters, J. Am. Ceram. Soc. 80(11) (1997) 2844-2852.
[29] B.D. Huey, R. Nath Premnath, S. Lee, N.A. Polomoff, High Speed SPM Applied for Direct Nanoscale Mapping of the Influence of Defects on Ferroelectric Switching Dynamics, J. Am. Ceram. Soc. 95(4) (2012) 1147-1162.
[30] J. Schultheiß, S. Checchia, H. Uršič, T. Frömling, J.E. Daniels, B. Malič, T. Rojac, J. Koruza, Domain wall-grain boundary interactions in polycrystalline $Pb(Zr_{0.7}Ti_{0.3})O_3$ piezoceramics, J. Eur. Ceram. Soc. 40(12) (2020) 3965-3973.
[31] X. Yan, M. Zheng, Y. He, M. Zhu, Y. Hou, Origin of superior dielectric and piezoelectric properties in $0.4Ba(Zr_{0.2}Ti_{0.8})O_3–0.6(Ba_{0.7}Ca_{0.3})TiO_3$ at intermediate grain sizes, J. Eur. Ceram. Soc. 40(12) (2020) 3936-3945.
[32] C. Hu, X. Meng, M.-H. Zhang, H. Tian, J.E. Daniels, P. Tan, F. Huang, L. Li, K. Wang, J.-F. Li, Q. Lu, W. Cao, Z. Zhou, Ultra-large electric field–induced strain in potassium sodium niobate crystals, Science Advances 6(13) (2020) eaay5979.
[33] C. Prescher, V.B. Prakapenka, DIOPTAS: a program for reduction of two-dimensional X-ray diffraction data and data exploration, High Pressure Research 35(3) (2015) 223-230.
[34] A. Hammersley, FIT2D: an introduction and overview, J European Synchrotron Radiation Facility Internal Report ESRF97HA02T 68 (1997) 58.
[35] B.H.J.J.o.a.c. Toby, EXPGUI, a graphical user interface for GSAS, Journal of Applied Crystallography 34(2) (2001) 210-213.
[36] R. Buttner, E.J.A.C.S.B.S.S. Maslen, Structural parameters and electron difference density in $BaTiO_3$, Acta Crystallogr., Sect. B: Struct. Sci 48(6) (1992) 764-769.
[37] G. Esteves, K. Ramos, C.M. Fancher, J.L. Jones, LIPRAS: Line-profile analysis software, Preprint at https://www.researchgate.net/publication/316985889_LIPRAS_Line-Profile_Analysis_Software (2017).
[38] L.Q. Chen, Phase-field method of phase transitions/domain structures in ferroelectric thin films: a review, J. Am. Ceram. Soc. 91(6) (2008) 1835-1844.
[39] C. Zhao, S. Gao, T. Yang, M. Scherer, J. Schultheiß, D. Meier, X. Tan, H.-J. Kleebe, L.-Q. Chen, J. Koruza, J. Rödel, Precipitation Hardening in Ferroelectric Ceramics, Adv. Mater. 33(36) (2021) 2102421.
[40] W.F. Liu, X.B. Ren, Large piezoelectric effect in Pb-free ceramics, Phys. Rev. Lett. 103(25) (2009) 257602.
[41] D.A. Hall, Review Nonlinearity in piezoelectric ceramics, Journal of Materials Science 36(19) (2001) 4575-4601.
[42] D. Damjanovic, M. Demartin, The Rayleigh law in piezoelectric ceramics, J. Phys. D: Appl. Phys. 29(7) (1996) 2057-2060.
[43] D. Damjanovic, Stress and frequency dependence of the direct piezoelectric effect in ferroelectric ceramics, J. Appl. Phys. 82(4) (1997) 1788-1797.
[44] Q.M. Zhang, H. Wang, N. Kim, L.E. Cross, Direct evaluation of domain-wall and intrinsic contributions to the dielectric and piezoelectric response and their temperature dependence on lead zirconate-titanate ceramics, J. Appl. Phys. 75(1) (1994) 454-459.
[45] D.A. Hall, A. Steuwer, B. Cherdhirunkorn, T. Mori, P.J. Withers, A high energy

synchrotron x-ray study of crystallographic texture and lattice strain in soft lead zirconate titanate ceramics, J. Appl. Phys. 96(8) (2004) 4245-4252.
[46] J.L. Jones, E.B. Slamovich, K.J. Bowman, Domain texture distributions in tetragonal lead zirconate titanate by x-ray and neutron diffraction, Journal of Applied Physics 97(3) (2005) 034113.
[47] T. Yamamoto, H. Igarashi, K. Okazaki, Dielectric, Electromechanical, Optical, and Mechanical Properties of Lanthanum-Modified Lead Titanate Ceramics, J. Am. Ceram. Soc. 66(5) (1983) 363-366.
[48] S.K. Choi, S.R. Kim, D.G. Choi, Effect of tetragonality ratio on photo-induced domain switching in poled $(Pb_{1-x}La_x)TiO_3$ ferroelectric ceramics, J. Mater. Sci. Mater. Electron. 11(8) (2000) 603-607.
[49] T. Leist, T. Granzow, W. Jo, J. Rödel, Effect of tetragonal distortion on ferroelectric domain switching: A case study on La-doped $BiFeO_3$–$PbTiO_3$ ceramics, J. Appl. Phys. 108(1) (2010).
[50] T. Leist, K.G. Webber, W. Jo, T. Granzow, E. Aulbach, J. Suffner, J. Rödel, Domain switching energies: Mechanical versus electrical loading in La-doped bismuth ferrite–lead titanate, J. Appl. Phys. 109(5) (2011).
[51] M.-H. Zhang, Y.-X. Liu, K. Wang, J. Koruza, J. Schultheiß, Origin of high electromechanical properties in $(K,Na)NbO_3$-based lead-free piezoelectrics modified with $BaZrO_3$, Physical Review Materials 4(6) (2020) 064407.
[52] G. Tutuncu, B. Li, K. Bowman, J.L. Jones, Domain wall motion and electromechanical strain in lead-free piezoelectrics: Insight from the model system $(1-x)Ba(Zr_{0.2}Ti_{0.8})O_3$–$x(Ba_{0.7}Ca_{0.3})TiO_3$ using in situ high-energy X-ray diffraction during application of electric fields, J. Appl. Phys. 115(14) (2014) 144104.
[53] J. Schultheiß, H. Kungl, J. Koruza, Influence of crystallographic structure on polarization reversal in polycrystalline ferroelectric/ferroelastic materials, J. Appl. Phys. 125(17) (2019) 174101.
[54] M. Majkut, J.E. Daniels, J.P. Wright, S. Schmidt, J. Oddershede, Electromechanical Response of Polycrystalline Barium Titanate Resolved at the Grain Scale, J. Am. Ceram. Soc. 100(1) (2017) 393-402.
[55] L. Daniel, D.A. Hall, P.J. Withers, A multiscale modelling analysis of the contribution of crystalline elastic anisotropy to intergranular stresses in ferroelectric materials, J. Phys. D: Appl. Phys. 47(32) (2014) 325303.
[56] Z. Zhao, K. Bowman, R.E. García, Modeling 180° Domain Switching Population Dynamics in Polycrystalline Ferroelectrics, J. Am. Ceram. Soc. 95(5) (2012) 1619-1627.
[57] D.A. Hall, A. Steuwer, B. Cherdhirunkorn, P.J. Withers, T. Mori, Micromechanics of residual stress and texture development due to poling in polycrystalline ferroelectric ceramics, J. Mech. Phys. Solids 53(2) (2005) 249-260.
[58] A. Pramanick, D. Damjanovic, J.E. Daniels, J.C. Nino, J.L. Jones, Origins of Electro-mechanical coupling in polycrystalline ferroelectrics during subcoercive electrical loading, J. Am. Ceram. Soc. 94(2) (2011) 293-309.
[59] C. Zhao, D. Hou, C.-C. Chung, H. Zhou, A. Kynast, E. Hennig, W. Liu, S. Li, J.L. Jones, Deconvolved intrinsic and extrinsic contributions to electrostrain in high performance, Nb-doped $Pb(ZrxTi1-x)O_3$ piezoceramics ($0.50 \leq x \leq 0.56$), Acta Mater. 158 (2018) 369-380.